Do all chlorophyll fluorescence emission wavelengths capture the spring recovery of photosynthesis in boreal evergreen foliage?

Zhang, Chao

2019-12

Zhang , C , Atherton , J , Penuelas , J , Filella , I , Kolari , P , Aalto , J , Ruhanen , H , Back , J & Porcar-Castell , A 2019 , ' Do all chlorophyll fluorescence emission wavelengths capture the spring recovery of photosynthesis in boreal evergreen foliage? ' , Plant, Cell and Environment , vol. 42 , no. 12 , pp. 3264-3279 . https://doi.org/10.1111/pce.13620

http://hdl.handle.net/10138/321552
https://doi.org/10.1111/pce.13620

unspecified
acceptedVersion

Zhang Chao (Orcid ID: 0000-0001-7327-9477)

Bäck Jaana (Orcid ID: 0000-0002-6107-667X)

Do all chlorophyll fluorescence emission wavelengths capture the spring recovery of photosynthesis in boreal evergreen foliage?

Running title: Spectral fluorescence in evergreens

Chao Zhang[1, 2, 3, *], Jon Atherton[1], Josep Peñuelas[2, 3], Iolanda Filella[2, 3], Pasi Kolari[4], Juho Aalto[4, 5], Hanna Ruhanen[6], Jaana Bäck[7], Albert Porcar-Castell[1,*]

[1]Optics of Photosynthesis Laboratory, Institute for Atmospheric and Earth System Research (INAR)/Forest Sciences/Viikki Plant Science Centre, Faculty of Agriculture and Forestry, University of Helsinki, PO Box 27, 00014 Helsinki, Finland.

[2]CREAF, Center for Ecological Research and Forestry Applications, Bellaterra 08193, Catalonia, Spain.

[3]CSIC, Global Ecology Unit CREAF-CSIC-UAB, Cerdanyola del Vallès 08193, Catalonia, Spain

[4]Department of Physics, University of Helsinki, PO Box 64, 00014 Helsinki, Finland.

[5]SMEAR II Station, University of Helsinki, Hyytiäläntie 124, Korkeakoski 35500, Finland

This article has been accepted for publication and undergone full peer review but has not been through the copyediting, typesetting, pagination and proofreading process which may lead to differences between this version and the Version of Record. Please cite this article as doi: 10.1111/pce.13620

[6]Natural Resources Institute Finland (Luke), Natural Resources and Bioproduction, Suonenjoki Unit, Juntintie 154, 77600 Suonenjoki, Finland.

[7]Department of Forest Sciences, University of Helsinki, PO Box 27, 00014 Helsinki, Finland.

[*]Corresponding authors: Chao Zhang, chao.x.zhang@helsinki.fi; Albert Porcar-Castell, joan.porcar@helsinki.fi

Abstract

Chlorophyll *a* fluorescence (ChlF) is closely related to photosynthesis and can be measured remotely using multiple spectral features as solar-induced fluorescence (SIF). In boreal regions, SIF shows particular promise as an indicator of photosynthesis; in part because of the limited variation of seasonal light absorption in these ecosystems. Seasonal spectral changes in ChlF could yield new information on processes such as sustained non-photochemical quenching (NPQ_S), but also disrupt the relationship between SIF and photosynthesis. We followed ChlF, functional and biochemical properties of *Pinus sylvestris* needles during the photosynthetic spring recovery period to answer; (1) how ChlF spectra change over seasonal timescales? (2) How pigments, NPQ_S and total PAR absorption drive changes of ChlF spectra? (3) Do all ChlF wavelengths track photosynthetic seasonality? We found seasonal ChlF variation in the red and far-red wavelengths, which was strongly correlated with NPQ_S, carotenoid content and photosynthesis (enhanced in the red), but not with PAR absorption. Furthermore, a rapid decrease in red/far-red ChlF ratio occurred in response to a cold spell, potentially relating to the structural reorganization of the photosystems. We conclude that all current SIF retrieval features can track seasonal

photosynthetic dynamics in boreal evergreens, but the full SIF spectra provides additional insight.

Key words: chlorophyll *a* fluorescence spectra, evergreen vegetation, F_{690}, F_{740}, leaf PAR absorption, *Pinus sylvestris*, PSI fluorescence, fluorescence ratio, sustained non-photochemical quenching (NPQ_S)

Summary statement

Chlorophyll fluorescence, a signal used to track photosynthesis at multiple scales, is distributed across a range of wavelengths. We followed chlorophyll fluorescence spectra during the photosynthetic spring recovery period for *Pinus sylvestris*. We found strong correlations between photosynthesis and fluorescence in both red and far-red emission wavelengths, and also minor changes in spectral shape related to short-term environmental stimuli.

Introduction

Chlorophyll *a* fluorescence (ChlF) of leaves, thylakoids and photosystems has been extensively used to study the organization, functioning, and acclimation of the photosynthetic light harvesting apparatus (Govindjee 1995; Baker 2008; Murchie & Lawson 2013; Porcar-Castell *et al.* 2014). ChlF can now be measured within discrete wavelengths from plant canopies, forest stands, and whole ecosystems with instrumentation on towers, drones, aircraft and satellites (Zarco-Tejada, Catalina, González & Martín 2013; Porcar-Castell *et al.* 2015; Rascher *et al.* 2015; Joiner, Yoshida, Guanter & Middleton 2016; Sun *et al.* 2017; Parazoo *et al.* 2018). Widely addressed as solar-induced fluorescence (SIF) by the remote sensing community, SIF opens up the study of photosynthesis at unprecedented scales (Frankenberg *et al.* 2011, 2014; Parazoo *et al.* 2014; Thum *et al.* 2017; Sun *et al.* 2018; Zhang, Guanter, Joiner, Song & Guan 2018; Zuromski *et al.* 2018). This capacity could not only serve to improve the current accuracy of global carbon budgets (Damm *et al.* 2015; Quéré

et al. 2018; Smith *et al.* 2018) but yield new understanding on the responses and feedbacks between terrestrial ecosystems and the environment, both critical milestones for the implementation of climate change mitigation and adaptation strategies (Smith *et al.* 2014; IPCC-SR15 2018).

Despite the mounting evidence of the strong link between SIF and gross primary productivity (GPP) accumulating from ground, airborne and satellite platforms (Guanter *et al.* 2014; Zarco-Tejada, González-Dugo & Fereres 2016; Migliavacca *et al.* 2017; Sun *et al.* 2017; Parazoo *et al.* 2018; Zuromski *et al.* 2018; Magney *et al.* 2019a), the physical and biological mechanisms that underpin the relationship and the potential wavelength-dependent information content in the SIF signal remain unclear (Porcar-Castell *et al.* 2014; Verrelst *et al.* 2016; Wieneke *et al.* 2018; Yang *et al.* 2018). This lack of understanding, is particularly acute for evergreen foliage, where the seasonal link between SIF and GPP involves processes other than changes in absorbed photosynthetically active radiation(APAR) which could decouple and add wavelength dependencies to the relationship between SIF and GPP.

In contrast to pulse-amplitude-modulation (PAM) ChlF measurements which integrate ChlF over a broad range of wavelengths, SIF is retrieved within narrow and discrete spectral bands around the red and far-red ChlF emission peaks (atmospheric oxygen absorption bands or solar Fraunhofer lines) (Alonso *et al.* 2007; Meroni *et al.* 2009). Accordingly, because the shape of the leaf-level ChlF spectra is driven by a combination of physical, physiological and biochemical factors (Magney *et al.* 2019b), it can be expected that the seasonal relationship between SIF and GPP would depend on retrieval wavelength, especially in boreal evergreen vegetation undergoing remarkable adjustments during the season.

A light use efficiency type model (Monteith 1972) becomes a convenient theoretical framework to introduce the physical and biological factors that couple (or decouple) SIF and GPP, and connect the leaf-level phenomenology to the spatial scale of remote sensing. The intensity of the SIF signal emitted from a leaf or a plant canopy at a given can be expressed as a function of four factors: 1) the incoming PAR, 2) the fraction of that PAR absorbed by the leaf or canopy (*A*), 3) the quantum yield of fluorescence with its associated emission wavelength (F), and 4) a wavelength dependent escape probability (f_{esc}) which accounts for the reabsorption of predominantly red ChlF photons by chlorophyll (Chl) molecules within the antenna, thylakoid, chloroplast, leaf or plant canopy (Buschmann 2007; Porcar-Castell *et al.* 2014; Romero, Cordon & Lagorio 2018; Yang & van der Tol 2018), as:

(Eqn. 1)

In similar terms, leaf or canopy level GPP can be expressed as:

(Eqn. 2)

where LUE corresponds to the photosynthetic light use efficiency in moles of CO_2 assimilated moles per mole of absorbed PAR photons. By combining equations (note that *A* and PAR cancel out), a simple theoretical relationship that links GPP to SIF can be obtained as:

——— ——— (Eqn. 3)

In this equation, widely applied to the interpretation of remotely sensed SIF data (Guanter *et al.* 2014; van der Tol, Berry, Campbell & Rascher 2014; Damm *et al.* 2015; Lee *et al.* 2015; Frankenberg & Berry 2018), physical factors (e.g. structure-dependent ChlF reabsorption) are embedded in the $1/f_{esc}$, and biological factors (e.g.

architecture and physiological state of the light reactions, alternative energy sinks, cyclic electron transport, photorespiration) are embedded F

Clearly, any seasonal changes in the strength of the factors above can potentially couple and decouple SIF and GPP (Porcar-Castell *et al.* 2014). In addition, any seasonal changes in the leaf-level wavelength properties of f_{esc} F can add wavelength dependencies to the link between SIF and GPP, something that remains to be characterized.

Seasonal changes in leaf Chl content, although usually modest in boreal evergreens (Öquist & Huner 2003; Ensminger *et al.* 2004; Porcar-Castell *et al.* 2008a), affect light absorption, and also f_{esc} ChlF reabsorption (Buschmann 2007). Similarly, structural changes at the level of chloroplast and thylakoid membrane, e.g. thylakoid grana unstacking and aggregation of Chl binding light harvesting complexes in overwintering evergreens (Öquist, Chow & Anderson 1992; Ruban, Johnson & Duffy 2012; Verhoeven 2014; Demmig-Adams, Muller, Stewart, Cohu & Adams 2015; Ruban 2016) could also contribute to the modulation of f_{esc} potentially affecting the spectral properties of SIF and its seasonal correlation to GPP.

is composed of at least two components: a highly dynamic component which responds to photochemical (PQ) and non-photochemical (NPQ) quenching of excitation energy in photosystem II (PSII) and that fluoresces in the red and far-red regions (Franck, Juneau & Popovic 2002; Palombi *et al.* 2011), and a component from photosystem I (PSI) assumed to remain stationary over the short term (Genty, Wonders & Baker 1990; Palombi *et al.* 2011; Pfündel, Klughammer, Meister & Cerovic 2013) that fluoresces predominantly in the near-infrared. Accordingly, if seasonal dynamics in sustained NPQ (NPQ_S) (Ottander, Campbell & Öquist 1995; Öquist & Huner 2003; Verhoeven 2014) quenched only the ChlF components from PSII, one

would expect NPQs to affect the spectral properties of . Similarly, differences in the patterns of seasonal photoinhibition of PSII (Ensminger *et al.* 2004; Murata, Takahashi, Nishiyama & Allakhverdiev 2007) and PSI reaction centres (Sonoike 2011; Huang, Yang, Hu & Zhang 2016) could also affect the ChlF spectra and its spectral dependency with photosynthesis.

In summary, although a strong seasonal coupling between PAM ChlF and photosynthesis has been widely reported for evergreen foliage (e.g. Ottander & Öquist 1991; Ensminger *et al.* 2004; Zarter, Demmig-Adams, Ebbert, Adamska & Adams 2006b; Soukupová *et al.* 2008; Kolari *et al.* 2014; Springer, Wang & Gamon 2017), the spectral dependency of the relationship remains unresolved.

The objective of the study was to characterize the seasonal variation of ChlF spectra for boreal evergreen Scots pine needles during the spring recovery of photosynthesis. Hence, we investigated if red and far-red wavelengths of ChlF were equally positioned to capture the spring recovery of photosynthesis. To do so we combined long-term and continuous *in situ* measurements of gas exchange, and PAM ChlF with repeated measurements of foliar pigment content, leaf total PAR absorption and spectral ChlF, spanning the full dynamic range of variation in photosynthetic capacity of Scots pine needles: from deeply downregulated foliage during winter, to fully functional foliage during peak growing season in summer**.**

Materials and methods

Study site and field sampling protocol

Measurements were conducted at Hyytiälä/SMEAR-II (Station for Measuring Forest Ecosystem-Atmosphere Relations) in Southern Finland (61°51´N, 24°17´E, 181m a. s.

l.) (Hari & Kulmala 2005), in a 52-year old Scots pine (*Pinus sylvestris* L.) stand with a dominant height of c. 18m. The study period (24th February - 20th July 2015) encompassed three biological seasons: end of winter (full dormant state), spring, and first half of summer (peak growing season).

The study combined continuous *in situ* measurements of micrometeorological variables, CO_2 exchange and PAM ChlF across four different trees (N= 4), with repeated point measurements of steady-state spectral ChlF at room temperature and pigment analysis across five trees (previous four plus one, N=5). Spectral ChlF was purposefully measured under standardized PAR so that it could serve as a proxy of $_F$ in Eqns 1 and 3, (i.e. APAR assumed constant). To avoid changing the needle cohort in the middle of the experiment, all measurements were conducted in the newest cohort of needles available at the start of the study period (developed in summer 2014). To avoid defoliation effects, several branches from the four topmost whorls were selected per tree and used for the repeated sampling of needles. Needles were sampled always before 10AM. Overall, the study included a total of 19 measuring points in addition to the continuous measurements (Fig. 1).

Continuous measurements of micrometeorological data and shoot CO_2 exchange

Air temperature (°C) (Pt100 sensor) and PAR ($^{-2}$ s^{-1}) (Li-190SZ, Li-Cor Inc., Lincoln, NE, USA) were measured right above the forest at 1 min intervals from sensors placed in a tall mast. The CO_2 exchange of pine shoots was measured in top canopy shoots 30-60 times per day using a system of automated dynamic chambers coupled to an infrared gas analyzer (Li-840, Li-Cor Inc., Lincoln, NE, USA) (see e.g. Aalto *et al.* 2014 for further details). Chambers remained open most of the time

exposing the studied shoots to ambient conditions and closed only during measurement. Fluxes were estimated from the change in CO_2 concentration during the first 40 s upon chamber closure (Kolari *et al.* 2012). Shoots with fully developed needles from 2014 were debudded prior to chamber installation to prevent new growth during the study period and for practical reasons. Total needle area inside the chamber was measured at the end of the study and used to calculate fluxes. A total of two to four chambers (N=2-4) were used during the study period from February 24th to July 20th in 2015 (Fig. S1a).

Direct comparison of noon LUE from chamber data (moles CO_2 assimilated /moles PAR absorbed) can be problematic in boreal conditions due to low PAR levels during the winter months. Accordingly, we decided to use here a simple model of photosynthesis (the optimal stomatal control model) (Hari, Mäkelä, Korpilahti & Holmberg 1986; Kolari, Lappalainen, Hänninen & Hari 2007) that allows robust estimation of photosynthetic parameters under ambient CO_2 concentrations, low light and low temperatures (Kolari *et al.* 2014). Two key photosynthetic parameters were estimated in a 3-day time window to capture the seasonal development in LUE; (1) (µmol CO_2 / µmol PAR), the slope of a linear function fitted to the photosynthetic light response with low incident PAR (<300 µmol m^{-2} s^{-1}) before noon (Fig. S1b; Kolari *et al.* 2014). Under constant leaf PAR absorption (Fig. S2), this parameter can be considered a measure of maximum photosynthetic LUE under low light. In addition, and since our spectral ChlF measurements were not conducted under low light, we also estimated (2) (m s^{-1}), the maximum rate of light-saturated photosynthesis per unit inter-cellular CO_2 concentration (Fig. S1c). This parameter can be considered a measure of light-saturated photosynthesis at optimal temperature, low vapour pressure deficit and ambient CO_2 concentration.

We normalized and parameters to their mean values between May 3rd and 23rd (see Fig. S1d,e). This is a common procedure in time-series analysis and serves to minimize the impact of systematic variability and emphasize the seasonal patterns in the data, which was our goal. The normalization period was selected in May as that was the time when all four chambers were simultaneously recording and the foliage was already photosynthetically active. Normalized unit-less values were then converted back to the original units by multiplying the normalized values by the respective means across all four chambers. The parameters and are used hereinafter as a measure of the seasonal spring recovery of photosynthesis.

Continuous measurements of PAM ChlF in situ

A Monitoring PAM system (MONI-PAM, Walz GmbH, and Germany) (Porcar-Castell, Pfündel, Korhonen & Juurola 2008b; Porcar-Castell 2011), equipped with 4 independent PAM fluorometers, was used to record the instantaneous fluorescence

$_M$), incoming PAR, and temperature every

$_M$ were assumed to correspond to minimal (F_o) and maximal (F_M) fluorescence and used to derive daily maximum quantum yield of PSII, F_V/F_M after Kitajima & Butler (1975), and to calculate quenching parameters NPQ_S and PQ_S after Porcar-castell (2011) as: $NPQ_S = F_{MR}/F_M - 1$ and $PQ_S = F_{MR}/F_o - F_{MR}/F_M$, where F_{MR} is the summer night reference obtained for those particular needles in the absence of NPQ_S. A decrease in PQ_S relative to summer levels was here interpreted in terms of photoinhibition of reaction centres (Porcar-Castell 2011). Finally, seasonal changes in

$_F$) we $_F = 0.1\ F_o/F_{MR}$ (Porcar-castell 2011, note the unfortunate typo in Eqn. $_M$ should be F_{MR}), which is

based on the assumption of a maximum fluorescence yield of 10% for PSII particles at the F_M state (Barber, Malkin & Telfer 1989). The four fluorometers were installed in top canopy branches pointing south.

Validation of ChlF measurements

For practical reasons, this study compared ChlF spectra of cut needles measured under standard conditions and at room temperature, with photosynthetic parameters (, , F_V/F_M, NPQ_S and PQ_S,) obtained from the field instrumentation. Accordingly, we wanted to test that our measurements at room temperature correctly represented the same physiological state as measurements carried out in the field. In addition, we wanted to ensure that our MONI-PAM system (which consistently supplied 48 light pulses per day to the same needles throughout the study period) was not introducing any long-term artefact. We used a Hansatech fluorometer (FMS-2, Hansatech Instruments Ltd., Kings Lynn, Norfolk, UK) to measure F_V/F_M both in the field and under standardized conditions indoors. During each sampling point, we placed a total of 25 dark-acclimation clips, distributed across the five study trees, and dark acclimated for at least 1 hour prior to measuring F_V/F_M. The same measurements were subsequently repeated at room temperature using collected needles instead. As expected, F_V/F_M obtained from the FMS-2 in the field was highly correlated with estimates from the MONI-PAM system (r=0.97, P<0.0001) (Fig. S3), denoting that the MONI-PAM system did not introduce any bias into the observed seasonal patterns. The small discrepancy between slopes is very likely due to differences in the colour of the measuring light as well as the ChlF detection range between instruments. Similarly, F_V/F_M measurements obtained with the FMS-2 fluorometer in field were found to be strongly correlated with those of detached needles at room temperature (r=0.94, P<0.0001) (Fig. S3),

suggesting that room temperature measurements did not introduce any major bias into the observed seasonal patterns in spectral ChlF.

Estimation of foliar pigment content

During each sampling point, five pairs of needles were randomly detached per each tree using the pre-selected top branches and needle cohort. Needles were sampled into cryotubes, immediately frozen at liquid nitrogen temperature using a portable dewar (CX-100, Taylor Wharton International LLC, Minnetonka, MN), and subsequently stored at -80 °C until extraction. Pigment analysis were conducted following Wellburn (1994) with dimethyl sulfoxide (DMSO; VWR Chemicals, 23500.322) as solvent. Frozen samples (75-100 mg) were first homogenized for 2 minutes at 30 Hz, using a bead mill (TissueLyser II Qiagen, Germany), stainless steel beads (4 mm) and microtubules (2 mL). Subsequently, 1.8 mL of DMSO was added to the homogenate and resuspended again at 30 Hz for 1 minute. Pigments were extracted in oven at 40 °C for 4 hours. Extracts were then centrifuged at 25000g for 5 minutes. Light absorption was measured at 649.1 nm, 665.1 nm and 480.0 nm, with a spectrophotometer (Shimadzu UV- 2401 PC), and subsequently used for estimation of Chl a, Chl b and total carotenoids (Wellburn 1994).

Measurements of leaf absorption

Needle PAR absorption ($A_{T(PAR)}$) was measured 8 times during the study period (N=5 biological replicates). We used the same spectrometer and LED light source described above connected to a 6 inch diameter integrating sphere (AdaptaSphere, LabSphere Inc, New Hampshire, UK), and applied the black spray method (Olascoaga, Mac Arthur, Atherton & Porcar-Castell 2016) to estimate $A_{T(PAR)}$. The black spray method

was inspired by earlier within-sphere measurements (Öquist, Hällgren & Brunes 1978; Idle & Proctor 1983) and purposefully developed to measure absorption in leaves with complex geometry, like needles, because it does not require mounting needles in the port of the integrating sphere and therefore there are no gap effects. Instead, samples are placed inside the sphere and hung from a white thread across the central plane (see illustrations in Olascoaga *et al.* 2016 for details). Prior to measurements, 5-6 needle pairs were separated and the resulting 10-12 needles sewed with a white thread and spaced at least 1 cm. The method consisted of three separate spectral measurements inside the sphere: 1) white thread alone (reference zero absorption, I_W), 2) white thread with needles (sample absorption, I_S), and 3) white thread with needles painted with a black spray of known absorption (Black sample, I_B). Conveniently, because the total surface area of the needles in steps 2) and 3) can be assumed to remain constant, this parameter cancels out and there is no need to estimate it. Total PAR absorption can then be computed by combining these three measurements with the known absorption of the black spray (A_{BLACK}), as:

——————— Eqn. 4

The mean value of A_T between 400 and 700nm was here used as an estimate of $A_{T(PAR)}$.

Room temperature measurements of leaf spectral ChlF

Leaf spectral ChlF (F in mW m^{-2} sr^{-1} nm^{-1}) was measured at room temperature using a FluoWat Clip (Image Processing Laboratory, University of Valencia, Spain) (Van Wittenberghe, Alonso, Verrelst, Moreno & Samson 2015) coupled with a powerful white LED (MJ-858, Magicshine, UK) and a radiometrically calibrated visible-near-

infrared spectrometer (FieldSpec, ASD-Panalytical, Boulder, CO). The spectrometer covers the spectral range between 325 and 1075 nm at a sampling interval of 1 nm and with a FWHM of 3.5 nm. The FluoWat clip has an optical window for input illumination (incidence angle of 45°) and a small aperture (at nadir view) to connect the optical fiber. The fiber field of view is 25° and the distance to sample is 1 cm, yielding an approximately circular target area of 0.22 cm radius. To obtain spectral ChlF, a 650 nm short-pass filter (Edmund Optics Ltd, UK, OD=4) was used to exclude 99.99% of radiation above 650 nm. The LED source supplies a PAR of c. 1200 µmol at the leaf surface as estimated with a PAR sensor (Licor LI150-A, Li-Cor Inc., Lincoln, NE, USA).

Needles were carefully arranged alongside each other to minimize the gap fraction and fixed with transparent tape to conform a needle mat (see Fig. 1). Rajewicz, Atherton, Alonso & Porcar-Castell (2019) recently compared the ChlF spectra of needles with different arrangements, and concluded that despite the fact that needle mats could slightly enhance reabsorption, they provided a higher replicability and reproducibility and were therefore a good solution to track temporal changes in spectral properties.

Needle mats were dark adapted at 10 °C for 1 hour and kept in the dark until measurements started in the FluoWat clip. After conducting a dark current measurement, the needle mat was placed in the FluoWat clip, recording was started, and an opaque aluminium foil placed between the light source and the FluoWat clip rapidly removed. Variations of spectral ChlF were recorded during two minutes at an integration time of 136 ms. The last ten spectra were averaged and used to estimate steady-state ChlF between 650 nm and 850 nm (F). Averaged spectra were further smoothed using a Savitzky-Golay filter (order=2, averaging interval=15) and cut to a

range of 660-780 nm where the signal was strongest. The resulting fluorescence spectra was used to estimate red (F_{690}) and far-red ChlF (F_{740}) and used to calculate an integrated steady-state ChlF between 660 and 780 nm ( ) for correspondence with the broadband PAM fluorescence parameter $_F$.

Statistical analyses

Mean values of four (gas exchange and Monitoring PAM fluorescence) or five (all other data) trees were used to conduct statistical analysis. Linear regression models and used to assess relationships between variables. All the analyses were conducted with R version 3.2.2 (R Core Development Team, 2015) and MATLAB version R2014a (MathWorks Inc. 2014).

Principal Component Analysis (PCA) was used to quantitatively assess the relative role of different components of variation in the spectral ChlF dataset. In particular, we wanted to quantify how much of the seasonal variation in spectral ChlF during the spring recovery of photosynthesis was related to principal components associated with changes in the intensity and how much was related to principal components associated with changes in the shape. T in the default mode ('prcomp' arguments; scale = FALSE and center = TRUE) was used to run a PCA on time series of the ChlF data-set. The analysis was focused on the 660-780 nm emission region to reduce impact of low signal-to-noise at wavelength limits.

Results

Seasonal changes in micrometeorological variables and photosynthetic parameters

Both temperature and PAR followed the typical annual pattern in boreal regions with PAR increasing faster and earlier than temperature (Fig. 2a). Daily mean temperatures in February (-1.7 °C) and March (0.6 °C) were higher by 6 and 4 °C, respectively, compared to the average for the period 1981-2010 (Pirinen *et al.* 2012). Fortunately, a cold spell took place on March 22nd with a daily mean temperature of -5.7 °C. On April 16th, a second cold spell took place with a mean temperature of 0.7 °C. These cold spells served to assess the responses of ChlF and photosynthetic parameters to a sudden decrease in temperature and were highlighted in figures reporting the time series.

Noon mean CO_2 fluxes (Fig. 2b) registered a clear seasonal pattern gradually increasing from April to June. Both (a measure of maximum LUE under low light) and (a measure of maximum photosynthetic rate) displayed similar seasonal patterns (Fig. 2c), gradually increasing from winter to summer. The effect of the cold spells on and parameters could not be distinguished.

Changes in the F_V/F_M and $_F$ (Fig. 2d) measured in the field with the MONI-PAM system also tracked the development of the spring recovery of photosynthesis, rapidly decreasing in response to the two cold spells and gradually recovering from winter to summer. Over the full spring recovery, $_F$ varied approximately by a factor of 2 from its minimum in early April to its maximum in June and July. Variations in F_V/F_M were further decomposed into PQ_S and NPQ_S components (Fig. 2e,f). NPQ_S presented larger seasonal variation decreasing from about 5 at the beginning of the study period to zero during summer. In contrast, PQ_S increased from values of about 3 at the

beginning of the study period to values of 4.5 during summer. Both NPQ_S and PQ_S consistently responded to both cold spells, increasing and decreasing, respectively.

Seasonal changes in pigment content and leaf absorption

No obvious seasonal patterns were observed in total Chl levels (Fig. 3a) although a slightly decreasing trend occurred during spring which reversed towards summer. This result was consistent with the time-series of total leaf PAR absorption ($A_{T(PAR)}$, Fig. S2) which did not display any seasonal pattern either with values ranging from 0.81 to 0.85. In contrast, seasonal changes were observed in Chl b (Fig. 3c), Chl a/b (Fig. 3d), carotenoid content (Fig. 3e) and Car/Chl ratios (Fig. 3f). During early spring, Chl a/b ratios were lower and carotenoid and Car/Chl ratios higher than during summer. No clear effects of the cold spells were seen in the pigments, except for Chl a/b which displayed higher levels after the second cold spell and Car/Chl which had a tendency to increase after the cold spells.

Seasonal variation in ChlF spectra

The ChlF spectra of pine needles measured at room temperature and at standard illumination (F , Fig. 4a-c) was used here as a proxy of variations in the spectrally resolved fluorescence yield. F experienced strong seasonal changes during the study period, mainly in terms of intensity but also in shape. For example, the red peak near 690nm was nearly absent during winter (Fig. 4a,b), but gradually reappeared towards summer (Fig. 4c). Both red (F_{690}) and far-red (F_{740}) ChlF (Fig. 4d) increased from early spring to summer with a larger change in F_{740}. Integrated ChlF (, Fig. 4e), used here for comparison with the spectrally averaged $_F$, presented a similar

seasonal pattern with the rest of photosynthetic parameters. Both $_F$ (Fig. 2d) and (Fig. 4e) varied seasonally by a factor of 2. The F_{690}/F_{740} ratio drastically decreased from 0.5 to 0.4 in response to the first cold spell, and did not reverse to 0.5 until several weeks later (Fig. 4f). Later on, the ratio decreased again to about 0.45 by the end of the study period, coinciding with the increase in total Chl (Fig. 3a) and F (Fig. 4d).

Principal component analysis

Three principal components explained 99.8% of the variation in ChlF spectra during the study period (Fig. 5). PC1 explained 98.8% of variance of ChlF spectra across the spring recovery (Fig. 5a) and exhibited a clear and similar seasonal pattern (Fig. 5b) to that of red, far-red, and integrated ChlF (Fig. 4d,e). The spectral weights and intensity of PC1 reflected the shape and seasonal variation in $_F$. In contrast, PC2 (Fig. 5c) explained only 0.8% of variance but its spectral weights presented a strong and wavelength dependent shape reflecting differences in red and far-red ChlF. PC2 potentially indicates seasonal changes in ChlF reabsorption (i.e. f_{esc} in Eqn.1), changes in energy redistribution between PSII and PSI, or changes in the emission spectra at the photosystem level. Remarkably, a drastic increase of PC2 (Fig. 5d) was detected upon the first cold spell (solid and vertical black line), and later on during summer when foliar Chl content tended to increase (Fig. 3a). Overall, the seasonal pattern of PC2 closely resembled the mirror image of F_{690}/F_{740} (Fig. 4f). PC3 explained only 0.2% of variance (Fig. 5e) and displayed no clear seasonal trend other than a sharp decrease at the end of April (Fig. 5f).

Seasonal correlations between photosynthetic parameters and spectral ChlF

Measurements of red, far-red and integral ChlF under standardized conditions were strongly correlated with field photosynthetic parameters (*r*: 0.81-0.83), (*r:* 0.84-0.86) and F_V/F_M (*r*: 0.87-0.89) (*P*<0.001 for all; Fig. 6 and Fig. S4). In contrast, no significant relationships between F_{690}/F_{740} and photosynthetic parameters were found. Red (F_{690}) and far-red (F_{740}) ChlF were strongly and negatively correlated also with leaf carotenoid content (*r*: -0.9 and -0.87, respectively) and NPQ_S (*r*: -0.86 and -0.83, respectively), and positively related with $_F$ (*r*: 0.73 and 0.71, respectively) and PQ_S (*r*: 0.74 and 0.71, respectively) (*P*<0.001 for all; Fig. 6 and Fig. S4). In fact, NPQ_S and leaf carotenoid content were the two factors that displayed the strongest (negative) correlation with the spring recovery of photosynthesis in terms of , , and F_V/F_M. No significant relationship was observed between red or far-red ChlF and total Chl or $A_{T(PAR)}$ (Fig. S4).

As for the principal components, PC1 was correlated strongly with F_V/F_M (*r* = 0.87), and negatively correlated with carotenoid, Car/Chl, and NPQ_S (*r*: -0.87 to -0.83), and had a significant but slightly lower relationship with $_F$ and PQ_S (*r* = 0.72) (*P*<0.001 for all; Fig. 6 and Fig. S4). PC2 was highly and negatively correlated with F_{690}/F_{740} (*r* = -0.92; *P*<0.001) but was not significantly correlated with $A_{T(PAR)}$ (*r* = 0.51) and total Chl (*r* = 0.37). Finally, PC3 was only marginally correlated with Chl a/b (*r* = 0.45; *P* = 0.06).

We also conducted a systematic assessment of the seasonal correlations between different ChlF emission wavelengths and photosynthetic parameters (Fig. 7). The results indicated that both red and far-red ChlF wavelengths were strongly correlated with the spring recovery of photosynthesis (*P*<0.001 for all), represented here by the photosynthetic parameters and (Fig. 7a), with red wavelengths displaying stronger

correlations than far-red wavelengths. Correlations were also stronger for , compared to across the whole spectral range, which is not surprising since our spectral measurements were conducted at high light. The strength of the correlation decreased between the two ChlF emission peak, with highest RMSE (data not shown). As expected, a wavelength dependency in the slope of ( ) vs. F was also observed (Fig. 7b), $_F$ was dependent on ChlF emission wavelengths. Positive intercepts of F vs. ( ) (Fig. 7c; with ranges of 0.15 to 0.95 mW m^{-2} sr^{-1} nm^{-1}) were obtained for both parameters and across wavelengths, indicating positive ChlF emission when photosynthetic gas exchange approaches zero.

Additionally, all the main ChlF emission wavelengths from 680 to 770 nm were well correlated with $_F$ (P<0.001 for all), and presented slightly stronger relationships in the red region than far-red (Fig. S5a). This was consistent with better correlations of ChlF with photosynthetic parameters in the red than in the far-red wavelengths (Fig. 7a). Further, when comparing F to , red wavelengths presented slightly lower correlations (Fig. S5b), reflecting that red ChlF fluorescence wavelengths account for a source of independent information not conveyed by broadband ChlF.

Discussion

We followed the spectral response of ChlF during the spring recovery of photosynthesis. We found an across wavelength increase in ChlF correlated with photosynthetic parameters, and additional subtler changes in spectral shape over time. Critically, photosystems in overwintering evergreens undergo major structural and biochemical adjustments during the non-photosynthetic season (Adams

& Demmig-Adams 1994; Ottander *et al.* 1995; Gilmore & Ball 2000; Ensminger *et al.* 2004; Verhoeven 2014), which were reflected in the variation of the measured ChlF spectra.

Seasonal variation in leaf-level ChlF spectra and its controls

We used PCA analysis to separate and quantify the relative roles of different components of variation in the seasonal ChlF dynamics of pine needles. We found that 98.8% of the seasonal variation in ChlF spectra of needles was explained by changes in ChlF level (PC1) with only a marginal 1% of variation associated with additional changes in shape (with PC2 explaining 0.8%). Factors contributing to these components of variation are discussed next.

Lack of correlation between F_{690}, F_{740} (and PC1), and total Chl content or $A_{T(PAR)}$ (Figs. 6 and S4) evidenced the minor role of PAR absorption in driving the seasonality of ChlF during the spring recovery. In the present study Chl content remained relatively stable (Fig. 3a). This is at odds with previous work where significant seasonal changes in Chl content have been observed in Scots pine needles (Ottander *et al.* 1995; Ensminger *et al.* 2004, Porcar-Castell *et al.* 2012), and other evergreen species (Wong & Gamon 2015). It is unclear why we observed such differences in pigments; but considering the alternative scenario where Chl did change during the season, and as the bulk of the spring recovery of ChlF in Scots pine needles has been shown to precede the summer increase in foliar Chl content by about two weeks (Porcar-Castell *et al.* 2008a), changes in leaf PAR absorption (A, Eqn.1) will likely remain of lesser importance in controlling the seasonality in leaf-level SI in evergreen conifers. We also did not find evidence of an inverse and persistent relationship between red/far-

red ratio and foliar Chl content across the study period (Figs. 6 and S4), as would follow from the general Chl reabsorption theory (Fig. 4A in Gitelson, Buschmann & Lichtenthaler 1999; Fig. 4 in Buschmann 2007). This result demonstrates that, in addition to foliar Chl content, other factors also influence the shape of the ChlF spectra.

Seasonal changes in both F_{690} and F_{740} (and PC1) were strongly related to seasonal variation in foliar carotenoid content, NPQs, and to a lesser extent PQs (Fig. 6). The mechanisms that drive NPQs in overwintering evergreens (understood as the sustained enhancement in the capacity for thermal dissipation of excitation energy), remain under intense investigation (Demmig-Adams & Adams 2006; Verhoeven 2014; Ruban 2016; Malnoë 2018). NPQs in evergreens has been associated to: the accumulation of carotenoids (especially zeaxanthin) relative to Chl (Adams & Demmig-Adams 1994; Ensminger *et al.* 2004; Zarter *et al.* 2006a; Porcar-Castell *et al.* 2012), the accumulation of damaged or non-functional PSII reaction centers coupled to a reduction in the PSII core D1 protein (Ottander *et al.* 1995; Ensminger *et al.* 2004; Ebbert, Adams, Mattoo, Sokolenko & Demmig-Adams 2005), the presence and accumulation of early-light induced proteins (Elips) with or without concomitant changes in minor antenna PsbS proteins (Ensminger *et al.* 2004; Ebbert *et al.* 2005; Zarter *et al.* 2006b; Verhoeven 2014), the aggregation of light-harvesting complexes of PSII (LHCII) (Horton *et al.* 1991; Ottander *et al.* 1995; Busch, Hüner & Ensminger 2007; Ruban 2018), and the unstacking of the thylakoid membrane (Demmig-Adams *et al.* 2015).

Reversible forms of NPQ, which operate in time scales of seconds to minutes, (e.g. energy-dependent or zeaxanthin-dependent quenching qE and qZ, respectively) (Verhoeven 2014; Malnoë 2018), are known to predominantly quench ChlF associated with PSII units with no apparent effect on PSI ChlF (Genty *et al.* 1990; Franck *et al.*

2002). As a result, because the ChlF contribution from PSI is much larger around the far-red peak (Genty *et al.* 1990; Pfündel 1998; Franck *et al.* 2002), an increase in qE or qZ results in a reduction in the red/far-red ChlF ratio (Agati, Mazzinghi, Fusi & Ambrosini 1995; Agati *et al.* 2000). If the PSI ChlF contribution would be also insensitive to NPQs, we would have expected a similar decrease in F_{690}/F_{740} in response to the seasonal accumulation of NPQs. This scenario was not fully supported by our observations because the extremes of variation in F_{690}/F_{740} ratio (observed during March, Fig. 4f) took place under comparable Chl and NPQs levels (Figs. 2f and 3a), suggesting that PSI ChlF contribution is dynamic at the seasonal scale.

Seasonal changes in the ChlF ratio are clearly driven by multiple controls. For example, F_{690}/F_{740} decreased from 0.5 to 0.4 in response to the first cold spell, along with an increase in NPQs (Fig. 2f) and in PC2 (Fig. 5d) which occurred under rather stable Chl content (Fig. 3a). This phenomena could denote a structural reorganization at the level of LHCII (increased reabsorption due to aggregation), or thylakoid membrane unstacking (promoting energetic connectivity between PSII and PSI units) accompanying the accumulation of NPQs. In fact, similar decreases in red/far-red ChlF ratio have been reported in response to reversible NPQ-induced oligomerization of LHCII complexes (Miloslavina *et al.* 2008; Jahns & Holzwarth 2012). Later on, in mid-May and July we registered a slight increase in foliar Chl content (Fig. 3a) accompanied by a decrease in the F_{690}/F_{740} ratio (Fig. 4f), and under rather stable NPQs (Fig. 2f) corresponding to the previous characterized relationship between leaf Chl content and the ChlF ratio (Gitelson *et al.* 1999). Overall, further experimental and modelling studies are needed to clarify the mechanisms that drive the dynamics in the ChlF spectra in overwintering evergreens.

Wavelength dependency between ChlF and photosynthesis

We found that all the main ChlF emission wavelengths (680-770 nm) were correlated with and capable of tracking the photosynthetic spring recovery in boreal evergreen foliage (Fig. 7a). This finding was consistent with the dominant role of NPQs in controlling the seasonal variability in the ChlF level across wavelengths (PC1; Fig. 5a,b). It is important to note however that the relative contributions of the variation in spectral shape (1% for PC2+PC3) and ChlF level (98.8% for PC1) to total seasonal variation in ChlF spectral properties could have been very different in a different species or under a different set of environmental conditions, encouraging further seasonal studies across other species and biomes.

Slightly higher correlations (Fig. 7a) and slopes (Fig. 7b) were found between red wavelengths of F and and . Similar results have been reported at the canopy scale based on model simulations (Verrelst *et al.* 2015; Liu *et al.* 2019) and experimental data (Cheng *et al.* 2013; Campbell *et al.* 2019; Magney *et al.* 2019a). At the leaf-level, the higher correlation in red wavelengths could point to interferences with the dynamics or PSI ChlF in the far-red wavelengths. In fact, the spectral shape of the intercept (Fig. 7c), which represents the background ChlF spectra at zero photosynthesis, had a high resemblance to the typical spectral shape of PSI ChlF, although the peak was slightly red-shifted (740 nm) compared to earlier studies in non-downregulated leaves of barley (722 nm) (Franck *et al.* 2002) or maize PSI particles (725-730 nm) (Croce, Dorra, Holzwarth & Jennings 2000). Further work to characterize and identify the drivers of this background ChlF signal, which may have important implications for interpretation of SIF data over boreal evergreen regions, is needed.

Implications at the larger scale

SIF is a promising methodology for the estimation of GPP dynamics in terrestrial ecosystems either using statistical methods based on Eqn. 3 (Guanter *et al.* 2014; Sun *et al.* 2017; Li *et al.* 2018), or by assimilation into the photosynthetic modules of land surface models (Lee *et al.* 2015; Thum *et al.* 2017; Macbean *et al.* 2018). SIF could be particularly useful for evergreen ecosystems by capturing part of the temporal dynamics of GPP that remains hidden to traditional reflectance-based vegetation indices due to low variation in greenness (Walther *et al.* 2016; Smith *et al.* 2018; Zuromski *et al.* 2018; Magney *et al.* 2019a; Nichol *et al.* 2019).

Overall, our results indicate that current Fraunhofer- and oxygen-based methods to retrieve SIF across different wavelengths in the red and near-infrared regions (Meroni *et al.* 2009; Lu, Cheng, Li & Tang 2018) have similar intrinsic potential to capture the leaf-level spring recovery of photosynthesis in boreal evergreen forests. Importantly, when upscaling from the leaf to the canopy and landscape level, the constancy $_{F}$ factor in Eqn. 3 will be further complicated by spatial variation in physiological factors caused by within canopy light and temperature gradients or species composition (Porcar-Castell *et al.* 2014; Sun *et al.* 2017). Similarly, canopy-level f_{esc} (Eqn. 3) will be also affected by seasonal dynamics in canopy structure related to the phenology of the multiple components in the ecosystem, including the understory (Majasalmi, Stenberg & Rautiainen 2017; Liu *et al.* 2019).

Conclusions

We demonstrated that red and far-red ChlF emission wavelengths were able to transmit the optical signature of the spring recovery of photosynthesis in boreal evergreen needles. The dynamics of the spectral signature were mediated by the complex and highly articulated process of sustained regulatory thermal dissipation or NPQ_S, which effectively quenches all ChlF wavelengths. Although changes in the shape of the ChlF spectra explained only a marginal proportion of the observed seasonality, the information content embedded in these changes could be highly informative. Specifically, the rapid decrease in the F_{690}/F_{740} ratio upon the first cold spell suggests that in addition to Chl content, F_{690}/F_{740} can also convey information on the structural organization in the thylakoid membrane in overwintering evergreens, which could help to better constrain the assimilation of SIF data into models of photosynthesis (Macbean *et al.* 2018; Raczka *et al.* 2019). Further investigations across species and scales will be required to fully characterize the information potentially embedded in the spectral dynamics of SIF, in support of multispectral SIF retrievals from towers, drones, airplanes as well as satellite missions such as current TROPOspheric Monitoring Instrument, TROPOMI, onboard Sentinel-5 (Guanter *et al.* 2015; Köhler *et al.* 2018) or future Fluorescence Explorer mission, FLEX (Drusch *et al.* 2017).

Acknowledgements: We acknowledge the financial support from the Academy of Finland (288039, 293443, 319211, 272041), the COST Action ES1309/OPTIMISE, the European Research Council Synergy grant SyG-2013-610028 IMBALANCE-P, the Spanish Government project CGL2016-79835-P, the Catalan Government project SGR 2014-274, and the Funds from the University of Helsinki (Grant 490116). HR was

supported by EU LIFE 12 ENV/FI/000409 Monimet. CZ gratefully acknowledges the support from the China Scholarship Council.

Conflict of interest: The authors have no conflicts of interest to declare.

Author Contribution: Albert Porcar-Castell, Jon Atherton, Iolanda Filella, Josep Peñuelas and Jaana Bäck conceived and designed the study; Chao Zhang and Albert Porcar-Castell carried out the optical measurements; Chao Zhang and Jon Atherton conducted the majority of the data analysis; Pasi Kolari estimated the photosynthetic parameters; Juho Aalto carried out and processed the field gas exchange data at SMEAR-II station; Hanna Ruhanen conducted the pigments analysis; Chao Zhang and Albert Porcar-Castell wrote the paper with contributions from all authors.

References

Aalto J., Kolari P., Hari P., Kerminen V.M., Schiestl-

(2014) New foliage growth is a significant, unaccounted source for volatiles in boreal evergreen forests. *Biogeosciences* **11**, 1331 1344.

Adams W.W. & Demmig-Adams B. (1994) Carotenoid composition and down regulation of photosystem II in three conifer species during the winter. *Physiologia Plantarum* **92**, 451 458.

Agati G., Cerovic Z.G. & Moya I. (2000) The effect of decreasing temperature up to chilling values on the in vivo F685/F735 chlorophyll fluorescence ratio in *Phaseolus vulgaris* and *Pisum sativum*: the role of the photosystem I

contribution to the 735 nm fluorescence band. *Photochemistry and Photobiology* **72**, 75 84.

Agati G., Mazzinghi P., Fusi F. & Ambrosini I. (1995) The F685/F730 chlorophyll fluorescence ratio as a tool in plant physiology: response to physiological and environmental factors. *Journal of Plant Physiology* **145**, 228 238.

Alonso L., Gómez-chova L., Vila-francés J., Amorós-lópez J., Guanter L., Calpe J. & Moreno J. (2007) Sensitivity analysis of the Fraunhofer Line Discrimination method for the measurement of chlorophyll fluorescence using a field spectroradiometer. *IEEE*, 3756 3759.

Baker N.R. (2008) Chlorophyll fluorescence: a probe of photosynthesis *in vivo*. *Annual review of plant biology* **59**, 89 113.

Barber J., Malkin S. & Telfer A. (1989) The origin of chlorophyll fluorescence *in vivo* and its quenching by the photosystem II reaction centre. *Philosophical Transactions of the Royal Society B: Biological Sciences* **323**, 227 239.

Busch F., Hüner N.P.A. & Ensminger I. (2007) Increased air temperature during simulated autumn conditions does not increase photosynthetic carbon gain but affects the dissipation of excess energy in seedlings of the evergreen conifer jack pine. *Plant Physiology* **143**, 1242 1251.

Buschmann C. (2007) Variability and application of the chlorophyll fluorescence emission ratio red/far-red of leaves. *Photosynthesis Research* **92**, 261 271.

Campbell P.K., Huemmrich K.F., Middleton E.M., Ward L.A., Julitta T., Daughtry

fluorescence associated with photosynthesis at leaf and canopy scales. *Remote Sensing* **11**, 1 36.

Cheng Y., Middleton E.M., Zhang Q., Huemmrich K.F., Campbell P.K.E., Corp

photochemical reflectance index for estimating gross primary production in a cornfield. *Remote Sensing* **5**, 6857 6879.

Croce R., Dorra D., Holzwarth A.R. & Jennings R.C. (2000) Fluorescence decay and spectral evolution in intact photosystem I of higher plants. *Biochemistry* **39**, 6341 6348.

Damm A., Guanter L., Paul-

Schaepman M.E. (2015) Far-red sun-induced chlorophyll fluorescence shows ecosystem-specific relationships to gross primary production: An assessment based on observational and modeling approaches. *Remote Sensing of Environment* **166**, 91 105.

Demmig-Adams B. & Adams W.W. (2006) Photoprotection in an ecological context: the remarkable complexity of thermal energy dissipation. *New Phytologist* **172**, 11 21.

Demmig-Adams B., Muller O., Stewart J.J., Cohu C.M. & Adams W.W. (2015) Chloroplast thylakoid structure in evergreen leaves employing strong thermal energy dissipation. *Journal of Photochemistry and Photobiology B: Biology* **152**, 357 366.

(2017) The FLuorescence EXplorer Mission Concept- Earth Explorer 8. *IEEE Transactions on Geoscience and Remote Sensing* **55**, 1273 1284.

Ebbert V., Adams W.W., Mattoo A.K., Sokolenko A. & Demmig-Adams B. (2005) Up-regulation of a photosystem II core protein phosphatase inhibitor and sustained

D1 phosphorylation in zeaxanthin-retaining, photoinhibited needles of overwintering Douglas fir. *Plant, Cell and Environment* **28**, 232 240.

Öquist G. (2004) Intermittent low temperatures constrain spring recovery of photosynthesis in boreal Scots pine forests. *Global Change Biology* **10**, 995 1008.

Franck F., Juneau P. & Popovic R. (2002) Resolution of the Photosystem I and Photosystem II contributions to chlorophyll fluorescence of intact leaves at room temperature. *Biochimica et Biophysica Acta - Bioenergetics* **1556**, 239 246.

relation to photosynthesis and retrieval. In *Reference Module in Earth Systems and Environmental Sciences: Comprehensive Remote Sensing, Elsevier, Oxford*. pp. 143 162. Elsevier.

Yokota T. (2011) New global observations of the terrestrial carbon cycle from GOSAT: Patterns of plant fluorescence with gross primary productivity. *Geophysical Research Letters* **38**, 1 6.

(2014) Prospects for chlorophyll fluorescence remote sensing from the Orbiting Carbon Observatory-2. *Remote Sensing of Environment* **147**, 1 12.

Genty B., Wonders J. & Baker N.R. (1990) Non-photochemical quenching of F_o in leaves is emission wavelength dependent: consequences for quenching analysis and its interpretation. *Photosynthesis Research* **26**, 133 139.

Gilmore A.M. & Ball M.C. (2000) Protection and storage of chlorophyll in

overwintering evergreens. *Proceedings of the National Academy of Sciences* **97**, 11098 11101.

Gitelson A.A., Buschmann C. & Lichtenthaler H.K. (1999) The chlorophyll fluorescence ratio F_{735} / F_{700} as an accurate measure of the chlorophyll content in plants. *Remote Sensing of Environment* **69**, 296 302.

Govindjee G. (1995) Sixty-three years since Kautsky: chlorophyll *a* fluorescence. *Australian Journal of Plant Physiology* **22**, 131 160.

Potential of the TROPOspheric Monitoring Instrument (TROPOMI) onboard the Sentinel-5 Precursor for the monitoring of terrestrial chlorophyll fluorescence. *Atmospheric Measurement Techniques* **8**, 1337 1352.

Global and time-resolved monitoring of crop photosynthesis with chlorophyll fluorescence. *Proceedings of the National Academy of Sciences*, 1 7.

Hari P. & Kulmala M. (2005) Station for measuring ecosystem-atmosphere relations (SMEAR II). *Boreal Environment Research* **10**, 351 322.

Hari P., Mäkelä A., Korpilahti E. & Holmberg M. (1986) Optimal control of gas exchange. *Tree Physiology* **2**, 169 175.

Horton P., Ruban A. V., Rees D., Pascal A.A., Noctor G. & Young A.J. (1991) Control of the light-harvesting function of chloroplast membranes by aggregation of the LHCII chlorophyll-protein complex. *FEBS Letters* **292**, 1 4.

Huang W., Yang Y.J., Hu H. & Zhang S.B. (2016) Seasonal variations in photosystem I compared with photosystem II of three alpine evergreen broad-leaf tree species. *Journal of Photochemistry and Photobiology B: Biology* **165**,

71 79.

Idle D.B. & Proctor C.W. (1983) An integrating sphere leaf chamber. *Plant, Cell and Environment* **6**, 437 439.

IPCC-SR15 (2018)

Jahns P. & Holzwarth A.R. (2012) The role of the xanthophyll cycle and of lutein in photoprotection of photosystem II. *Biochimica et Biophysica Acta - Bioenergetics* **1817**, 182 193.

Joiner J., Yoshida Y., Guanter L. & Middleton E.M. (2016) New methods for the retrieval of chlorophyll red fluorescence from hyperspectral satellite instruments: simulations and application to GOME-2 and SCIAMACHY. *Atmospheric Measurement Techniques* **9**, 3939 3967.

Kitajima M. & Butler W.L. (1975) Quenching of chlorophyll fluorescence and primary photochemistry in chloroplasts by dibromothymoquinone. *Biochimica et Biophysica Acta* **376**, 105 115.

Köhler P., Frankenberg C., Magney T.S., Guanter L., Joiner J. & Landgraf J. (2018) Global retrievals of solar-induced chlorophyll fluorescence with TROPOMI: first results and intersensor comparison to OCO-2. *Geophysical Research Letters* **45**, 10,456-10,463.

(2012) Evaluation of accuracy in measurements of VOC emissions with dynamic chamber system. *Atmospheric Environment* **62**, 344 351.

Kolari P., Chan T., Porcar-Castell A., Bäck J., Nikinmaa E. & Juurola E. (2014) Field and controlled environment measurements show strong seasonal acclimation in photosynthesis and respiration potential in boreal Scots pine. *Frontiers in Plant*

Science **5**, 717.

Kolari P., Lappalainen H.K., Hänninen H. & Hari P. (2007) Relationship between temperature and the seasonal course of photosynthesis in Scots pine at northern timberline and in southern boreal zone. *Tellus B: Chemical and Physical Meteorology* **59B**, 542 552.

Lee J.-E., Berry J.A., van der Tol C.

C. (2015) Simulations of chlorophyll fluorescence incorporated into the Community Land Model version 4. *Global Change Biology* **21**, 3469 3477.

n A. (2018) Solar-induced chlorophyll fluorescence is strongly correlated with terrestrial photosynthesis for a wide variety of biomes: First global analysis based on OCO-2 and flux tower observations. *Global Change Biology*, 1 19.

Liu W., Atherton J., Mõttus M., Gastellu-Etchegorry J.P., Malenovský Z., Raumonen

-Castell A. (2019) Simulating solar-induced chlorophyll fluorescence in a boreal forest stand reconstructed from terrestrial laser scanning measurements. *Remote Sensing of Environment* **in press**.

Lu X., Cheng X., Li X. & Tang J. (2018) Opportunities and challenges of applications of satellite-derived sun-induced fluorescence at relatively high spatial resolution. *Science of the Total Environment* **619 620**, 649 653.

Macbean N., Maignan F., Baco

(2018) Strong constraint on modelled global carbon uptake using solar-induced chlorophyll fluorescence data. *Scientific reports*, 1 12.

Magney T.S., Bowling D.R., Logan B., Grossmann K., Stutz J., Blanken

Frankenberg C. (2019a) Mechanistic evidence for tracking the seasonality of

photosynthesis with solar-induced fluorescence. *Proceedings of the National Academy of Sciences* **116**, 11640 11645.

-

Castell A. (2019b) Disentangling changes in the spectral shape of chlorophyll fluorescence: Implications for remote sensing of photosynthesis. *Journal of Geophysical Research: Biogeosciences* **124**, 1 17.

Majasalmi T., Stenberg P. & Rautiainen M. (2017) Comparison of ground and satellite-based methods for estimating stand-level fPAR in a boreal forest. *Agricultural and Forest Meteorology* **232**, 422 432.

Malnoë A. (2018) Photoinhibition or photoprotection of photosynthesis? Update on the (newly termed) sustained quenching component qH. *Environmental and Experimental Botany* **154**, 123 133.

Meroni M., Rossini M., Guanter L., Alonso L., Rascher U., Colombo R. & Moreno J. (2009) Remote sensing of solar-induced chlorophyll fluorescence: review of methods and applications. *Remote Sensing of Environment* **113**, 2037 2051.

Migliavacca M., Perez-Priego O., Rossini M., El-Madany T.S., Moreno G., van der

control the relationship between photosynthetic CO_2 uptake and far-red sun-induced fluorescence in a Mediterranean grassland under different nutrient availability. *New Phytologist* **214**, 1078 1091.

Holzwarth A.R. (2008) Far-red fluorescence: A direct spectroscopic marker for LHCII oligomer formation in non-photochemical quenching. *FEBS Letters* **582**, 3625 3631.

Monteith J.L. (1972) Solar radiation and productivity in tropical ecosystems. *Journal of Applied Ecology* **9**, 747 766.

Murata N., Takahashi S., Nishiyama Y. & Allakhverdiev S.I. (2007) Photoinhibition of photosystem II under environmental stress. *Biochimica et Biophysica Acta - Bioenergetics* **1767**, 414 421.

Murchie E.H. & Lawson T. (2013) Chlorophyll fluorescence analysis: a guide to good practice and understanding some new applications. *Journal of Experimental Botany* **64**, 3983 3998.

Nichol C., Drolet G., Porcar-

Atherton J. (2019) Seasonal solar induced chlorophyll fluorescence and photosynthesis in a boreal Scots pine canopy. *Remote Sensing* **11**, 273.

Olascoaga B., Mac Arthur A., Atherton J. & Porcar-Castell A. (2016) A comparison of methods to estimate photosynthetic light absorption in leaves with contrasting morphology. *Tree Physiology* **36**, 368 379.

Öquist G., Chow W.S. & Anderson J.M. (1992) Photoinhibition of photosynthesis represents a mechanism for the long-term regulation of photosystem II. *Planta* **186**, 450 460.

Öquist G., Hällgren J.E. & Brunes L. (1978) An apparatus for measuring photosynthetic quantum yields and quanta absorption spectra of intact plants. *Plant, Cell and Environment* **1**, 21 27.

Öquist G. & Huner N.P.A. (2003) Photosynthesis of overwintering evergreen plants. *Annual Review of Plant Biology* **54**, 329 355.

Ottander C., Campbell D. & Öquist G. (1995) Seasonal changes in photosystem II organisation and pigment composition in *Pinus sylvestris*. *Planta* **197**, 176 183.

Ottander C. & Öquist G. (1991) Recovery of photosynthesis in winter-stressed Scots pine. *Plant, Cell and Environment* **14**, 345 349.

Palombi L., Cecchi G., Lognoli D., Raimondi V., Toci G. & Agati G. (2011) A retrieval algorithm to evaluate the photosystem I and photosystem II spectral contributions to leaf chlorophyll fluorescence at physiological temperatures. *Photosynthesis research* **108**, 225 239.

(2018) Spring photosynthetic onset and net CO_2 uptake in Alaska triggered by landscape thawing. *Global Change Biology*, 3416 3435.

Parazoo N.C., Bowman K., Fisher J.B., Frankenberg C., Jones D.B.A., Cescatti

satellite fluorescence and vegetation models. *Global Change Biology* **20**, 3103 3121.

Pfündel E. (1998) Estimating the contribution of photosystem I to leaf chlorophyll fluorescence. *Photosynthesis Research* **56**, 185 195.

Pfündel E.E., Klughammer C., Meister A. & Cerovic Z.G. (2013) Deriving fluorometer-specific values of relative PSI fluorescence intensity from quenching of F_0 fluorescence in leaves of *Arabidopsis thaliana* and *Zea mays*. *Photosynthesis research* **114**, 189 206.

Pirinen P., Simola H., Aalto J., Kaukoranta J.-P., Karlsson P. & Ruuhela R. (2012) *Tilastoja suomen ilmastosta 1981-2010. (Climatological statistics of Finland 1981 2010)*.

Porcar-Castell A. (2011) A high-resolution portrait of the annual dynamics of photochemical and non-photochemical quenching in needles of *Pinus sylvestris*.

Physiologia Plantarum **143**, 139 153.

Porcar-Castell A., Mac Arthur A., Rossini M., Eklundh L., Pacheco-Labrador J.,

remote-sensing and ecosystem CO_2 flux measurements in Europe. *Biogeosciences* **12**, 6103 6124.

Porcar-Castell A., Garcia-Plazaola J.I., Nichol C.J., Kolari P., Olascoaga B.,

between the photochemical reflectance index and photosynthetic light use efficiency. *Oecologia* **170**, 313 323.

Porcar-Castell A., Juurola E., Ensminger I., Berninger F., Hari P. & Nikinmaa E. (2008a) Seasonal acclimation of photosystem II in *Pinus sylvestris*. II. Using the rate constants of sustained thermal energy dissipation and photochemistry to study the effect of the light environment. *Tree physiology* **28**, 1483 1491.

Porcar-Castell A., Pfündel E., Korhonen J.F.J. & Juurola E. (2008b) A new monitoring PAM fluorometer (MONI-PAM) to study the short- and long-term acclimation of photosystem II in field conditions. *Photosynthesis research* **96**, 173 179.

Porcar-Castell A., Tyystjärvi E., Atherton J., van der Tol C., Flexas J., Pfündel

for remote sensing applications: mechanisms and challenges. *Journal of Experimental Botany* **65**, 4065 4095.

Adrie and B.Z. (2018) Global Carbon Budget 2018. *Earth System Science Data* **10**, 2141 2194.

Raczka B., Porcar Castell A., Magney T., Lee J.E., Köhler P., Fr
Bowling D.R. (2019) Sustained non photochemical quenching shapes the seasonal pattern of solar induced fluorescence at a high elevation evergreen forest. *Journal of Geophysical Research: Biogeosciences* **124**.

Rajewicz P., Atherton J., Alonso L. & Porcar-Castell A. (2019) Leaf-level spectral fluorescence measurements: comparing methodologies for broadleaves and needles. *Remote Sensing* **11**, 1 20.

(2015) Sun-induced fluorescence a new probe of photosynthesis: First maps from the imaging spectrometer *HyPlant*. *Global Change Biology* **21**, 4673 4684.

Romero J.M., Cordon G.B. & Lagorio M.G. (2018) Modeling re-absorption of fluorescence from the leaf to the canopy level. *Remote Sensing of Environment* **204**, 138 146.

Ruban A. V. (2018) Light harvesting control in plants. *FEBS Letters* **592**, 3030 3039.

Ruban A. V (2016) Nonphotochemical chlorophyll fluorescence quenching: mechanism and effectiveness in protecting plants from photodamage. *Plant physiology* **170**, 1903 1916.

Ruban A. V, Johnson M.P. & Duffy C.D.P. (2012) The photoprotective molecular switch in the photosystem II antenna. *Biochimica et Biophysica Acta* **1817**, 167 181.

F.N. (2014) Agriculture, Forestry and Other Land Use (AFOLU). *Climate Change 2014: Mitigation of Climate Change. Contribution of Working Group III to the Fifth Assessment Report of the Intergovernmental Panel on Climate*

Change, 811 922.

M.E. (2018) Chlorophyll fluorescence better captures seasonal and interannual gross primary productivity dynamics across dryland ecosystems of southwestern North America. *Geophysical Research Letters* **45**, 748 757.

Sonoike K. (2011) Photoinhibition of Photosystem I. *Physiologia Plantarum* **142**, 56 64.

Nedbal L. (2008) Annual variation of the steady-state chlorophyll fluorescence emission of evergreen plants in temperate zone. *Functional Plant Biology* **35**, 63 76.

Springer K.R., Wang R. & Gamon J.A. (2017) Seasonal patterns of photosynthesis, fluorescence, and reflectance indices in boreal trees. *Remote Sensing* **9**, 1 18.

Sun Y., Frankenberg C., Jung M., Joiner J., Guanter L., Köhler P. & Magney T. (2018) Overview of Solar-Induced chlorophyll Fluorescence (SIF) from the Orbiting Carbon Observatory-2: Retrieval, cross-mission comparison, and global monitoring for GPP. *Remote Sensing of Environment* **209**, 808 823.

Sun Y., Frankenberg C., Wood J.D., Schimel D.S., Jung M., Guanter L (2017) OCO-2 advances photosynthesis observation from space via solar-induced chlorophyll fluorescence. *Science* **358**.

(2017) Modelling sun-induced fluorescence and photosynthesis with a land surface model at local and regional scales in northern Europe. *Biogeosciences* **14**, 1969 1987.

van der Tol C., Berry J.A., Campbell P.K.E. & Rascher U. (2014) Models of fluorescence and photosynthesis for interpreting measurements of solar-induced chlorophyll fluorescence. *Journal of Geophysical Research: Biogeosciences* **119**, 2312 2327.

Verhoeven A. (2014) Sustained energy dissipation in winter evergreens. *New Phytologist* **201**, 57 65.

Verrelst J., Rivera J.P., van der Tol C., Magnani F., Mohammed G. & Moreno J. (2015) Global sensitivity analysis of the SCOPE model: What drives simulated canopy-leaving sun-induced fluorescence? *Remote Sensing of Environment* **166**, 8 21.

Verrelst J., van der Tol C., Magnani F., Sabater N., Rivera J.P., Mohammed G. & Moreno J. (2016) Evaluating the predictive power of sun-induced chlorophyll fluorescence to estimate net photosynthesis of vegetation canopies: a SCOPE modeling study. *Remote Sensing of Environment* **176**, 139 151.

(2016) Satellite chlorophyll fluorescence measurements reveal large-scale decoupling of photosynthesis and greenness dynamics in boreal evergreen forests. *Global Change Biology* **22**, 2979 2996.

Wellburn A.R. (1994) Spectral determination of chlorophylls a and b, as well as total carotenoids, using various solvents with spectrophotometers of different resolution. *Journal of Plant Physiology* **144**, 307 313.

Wieneke S., Burkart A., Cendrero-Mateo M.P., Julitta T., Rossini M., Schickling

-induced fluorescence

at sub-daily to seasonal scales. *Remote Sensing of Environment* **219**, 247 258.

Van Wittenberghe S., Alonso L., Verrelst J., Moreno J. & Samson R. (2015) Bidirectional sun-induced chlorophyll fluorescence emission is influenced by leaf structure and light scattering properties - A bottom-up approach. *Remote Sensing of Environment* **158**, 169 179.

Wong C.Y.S. & Gamon J.A. (2015) The photochemical reflectance index provides an optical indicator of spring photosynthetic activation in evergreen conifers. *New Phytologist* **206**, 196 208.

Yang P. & van der Tol C. (2018) Linking canopy scattering of far-red sun-induced chlorophyll fluorescence with reflectance. *Remote Sensing of Environment* **209**, 456 467.

U. (2018) Using reflectance to explain vegetation biochemical and structural effects on sun-induced chlorophyll fluorescence. *Remote Sensing of Environment*.

Zarco-Tejada P.J., Catalina A., González M.R. & Martín P. (2013) Relationships between net photosynthesis and steady-state chlorophyll fluorescence retrieved from airborne hyperspectral imagery. *Remote Sensing of Environment* **136**, 247 258.

Zarco-Tejada P.J., González-Dugo M. V. & Fereres E. (2016) Seasonal stability of chlorophyll fluorescence quantified from airborne hyperspectral imagery as an indicator of net photosynthesis in the context of precision agriculture. *Remote Sensing of Environment* **179**, 89 103.

Zarter C.R., Adams W.W., Ebbert V., Cuthbertson D.J., Adamska I. & Demmig-Adams B. (2006a) Winter down-regulation of intrinsic photosynthetic capacity

coupled with up-regulation of Elip-like proteins and persistent energy dissipation in a subalpine forest. *New Phytologist* **172**, 272 282.

Zarter C.R., Demmig-Adams B., Ebbert V., Adamska I. & Adams W.W. (2006b) Photosynthetic capacity and light harvesting efficiency during the winter-to-spring transition in subalpine conifers. *New Phytologist* **172**, 283 292.

Zhang Y., Guanter L., Joiner J., Song L. & Guan K. (2018) Spatially-explicit monitoring of crop photosynthetic capacity through the use of space-based chlorophyll fluorescence data. *Remote Sensing of Environment* **210**, 362 374.

Zuromski L.M., Bowling D.R., Köhler P., Frankenberg C., Goulden M.L., Blanken P.D. & Lin J.C. (2018) Solar-induced fluorescence detects interannual variation in gross primary production of coniferous forests in the western United States. *Geophysical Research Letters* **45**, 7184 7193.

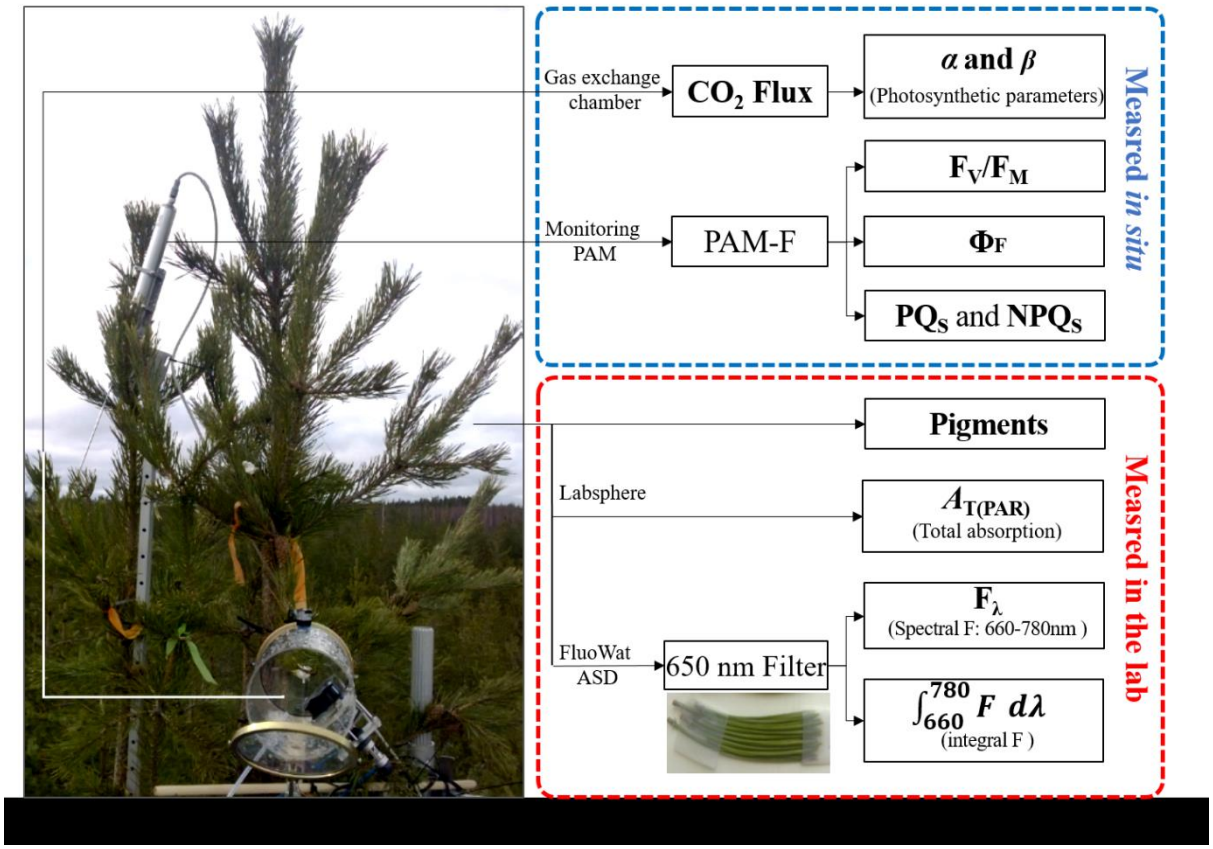

Fig. 1. Measurement rationale during the spring recovery of 2015 in *Pinus sylvestris*.

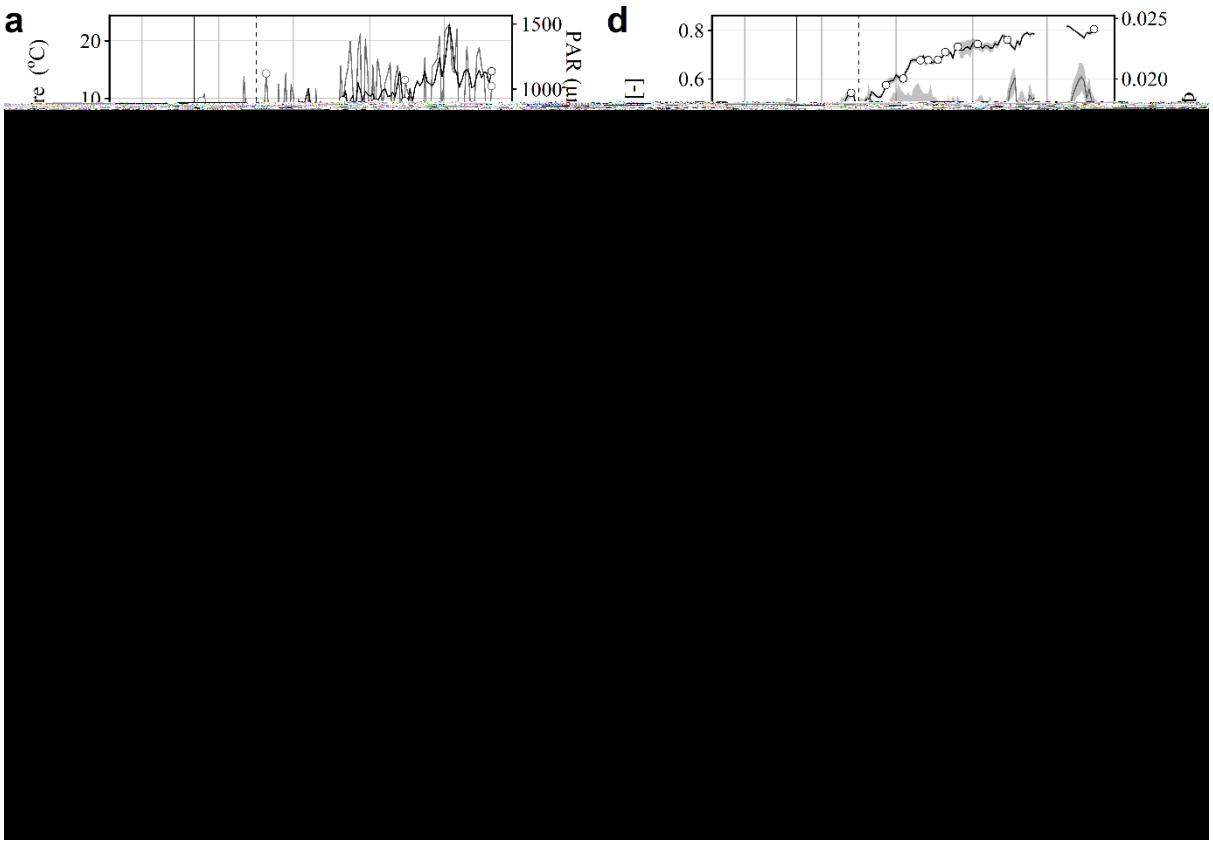

Fig. 2. Seasonal variation of meteorological and photosynthetic parameters.